Supporting Information for

Rotational 3D printing technique with pixel compensation for enhanced dynamic performance

This PDF file includes:

Figures S1 to S7

Other supporting materials for this manuscript include the following:

Movies S1 to S4

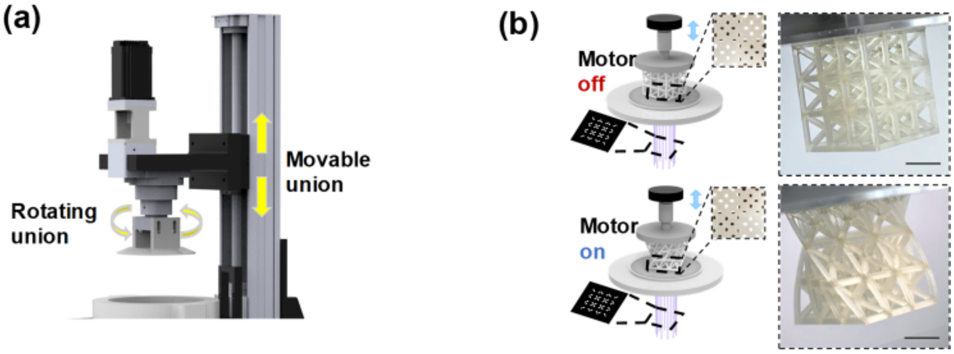

Fig. S1. Rotational printing platform assembly and operational modes. a) Schematic of the rotating union connecting the motor shaft to the build platform. b) Illustration of the motor control states (off/on), demonstrating the system's ability to switch between conventional static DLP printing (motor off) and rotational 3D printing (R3DP) mode (motor on). Scale bar, 1cm.

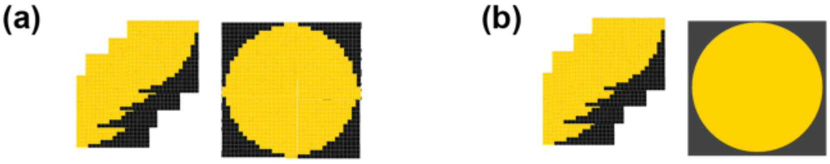

Fig. S2. Schematic illustration comparing the voxel deposition and surface formation mechanisms in conventional DLP versus R3DP. a) The fixed alignment of pixels from the projector leads to the cumulative “stair-stepping” artifacts at curved surfaces due to the misalignment between discrete pixel boundaries and the ideal contour. This results in pronounced edge roughness and geometric inaccuracies. b) The concomitant radial displacement compensates for missing edge pixels, resulting in a smooth surface that closely approximates the intended digital geometry.

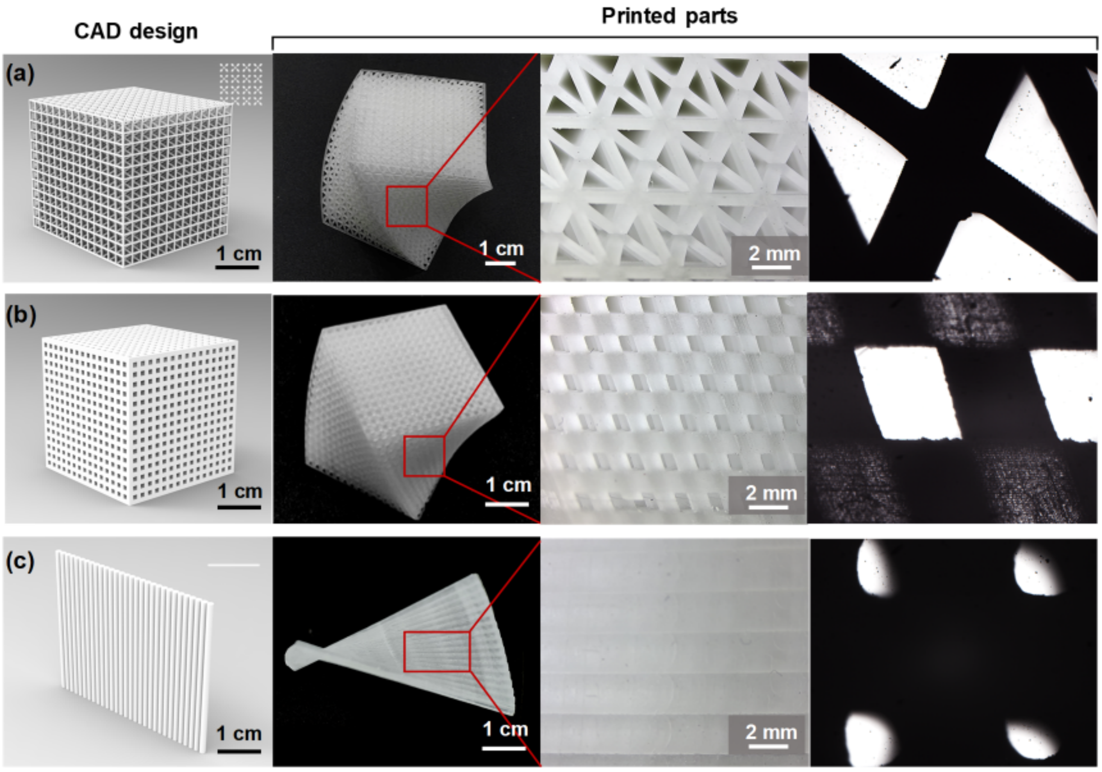

Fig. S3. Expanded library of complex, centrally symmetric architectures fabricated via the rotational 3D printing (R3DP) platform from a single sliced file.The ability to produce such intricate and varied geometries from one initial slice file underscores the unparalleled design freedom and manufacturing versatility of the R3DP technique.

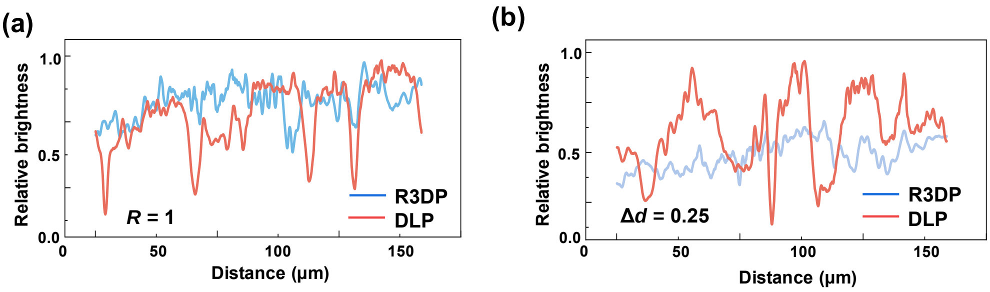

Fig. S4. Quantitative comparison of edge uniformity between DLP and R3DP printed structures. The intensity profiles quantitatively demonstrate that the DLP-printed edge exhibits severe fluctuations, directly corresponding to the pronounced pixelation artifacts and surface roughness. In stark contrast, the R3DP-printed edge maintains a near-uniform intensity profile, confirming the significant smoothing effect achieved through layer-wise rotational displacement.

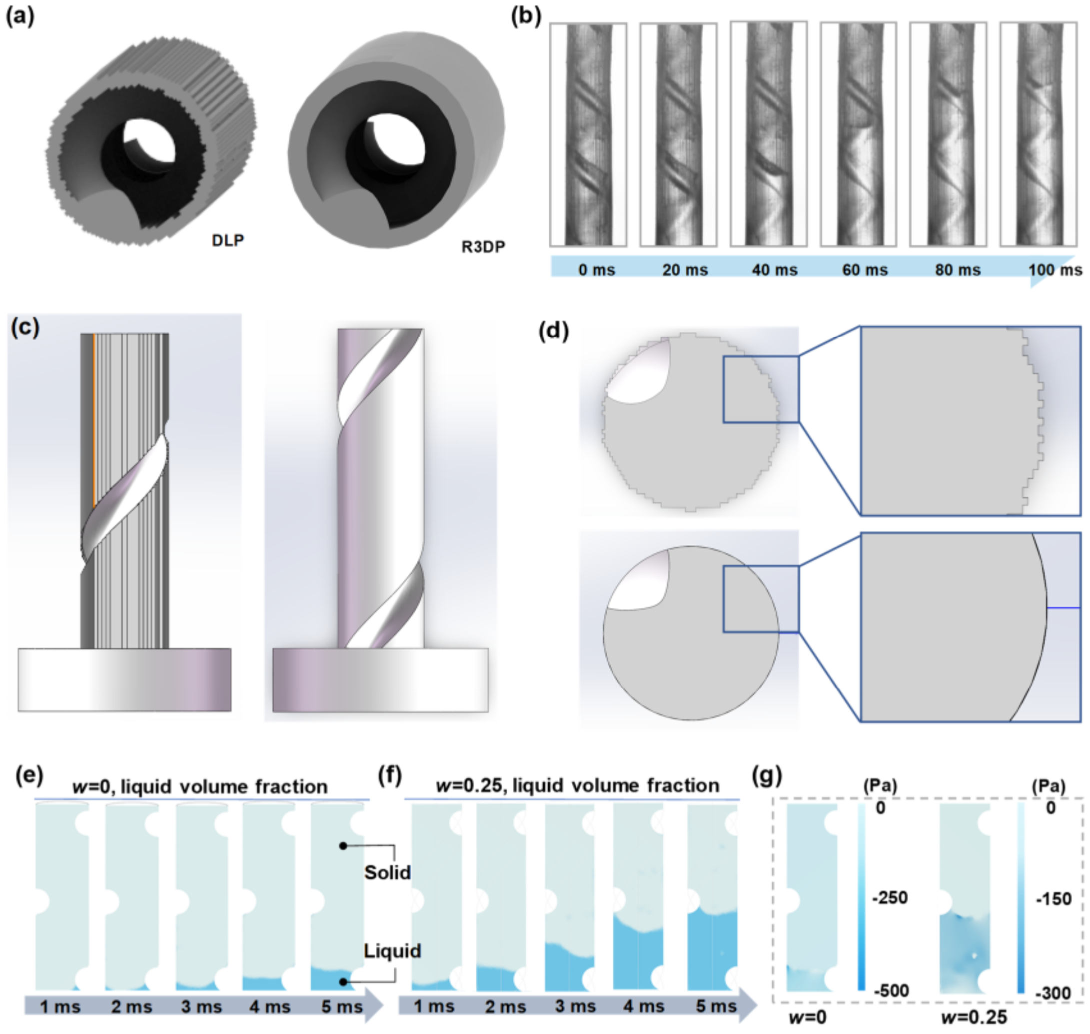

Fig. S5. Comparative visualization of capillary flow dynamics in helical microchannels. Side-view snapshots of the liquid-air meniscus during capillary rise within microchannels fabricated by conventional DLP printing (ω = 0) and our R3DP technique (ω = 0.25). The DLP-printed channel exhibits significant flow front distortion and pinning (yellow arrows) due to surface roughness from pixelation artifacts. In contrast, the R3DP-fabricated channel demonstrates a uniform, coherent meniscus progression, indicative of superior surface smoothness and hydrodynamic performance.

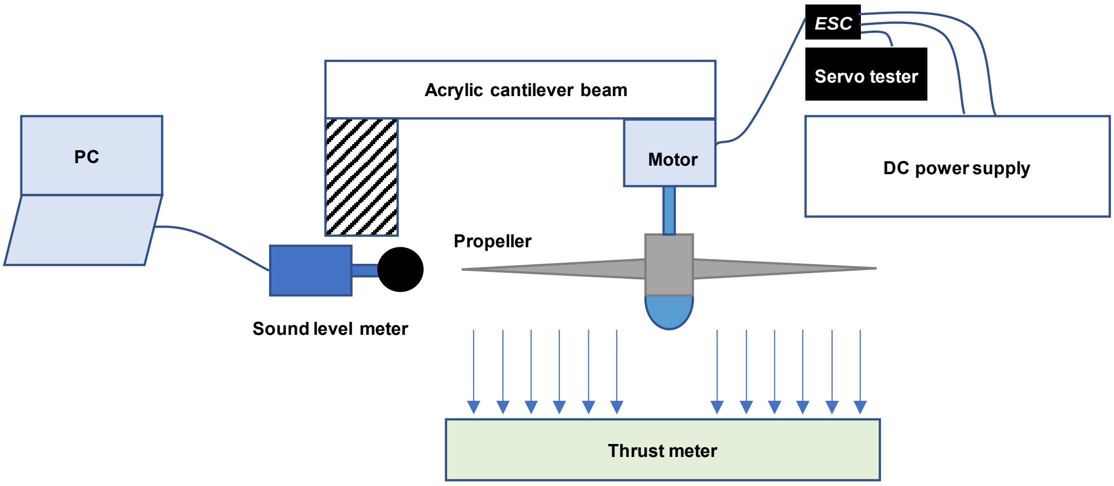

Fig. S6. Schematic of the experimental setup for propeller thrust and acoustic performance characterization. The propeller is mounted on a brushless motor, which is fixed to a thrust stand equipped with a high-precision load cell for force measurement. The rotational speed of the motor is precisely controlled by an electronic speed controller (ESC). A sound level meter is positioned at a standardized distance from the propeller to record the acoustic emissions.

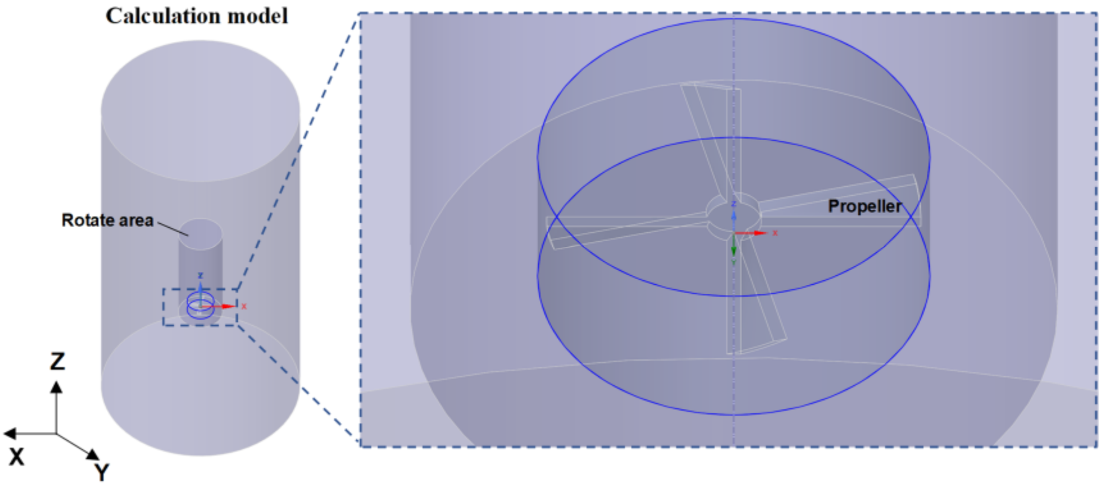

Fig. S7. Numerical simulation model for propeller aerodynamics using the Moving Reference Frame (MRF) approach. Schematic of the computational domain established for the CFD analysis, showing the stationary outer fluid field and the inner rotating domain enclosing the propeller. Boundary conditions including velocity inlet, pressure outlet, and wall conditions are annotated.

Movie. S1 R3DP enables continuous triple-spring fabrication from a single sliced file.

Movie. S2 Capillary filling process in R3DP-fabricatedspring microchannels.

Movie. S3 Comparative capillary flow dynamics in DLP-vs. R3DP-fabricated microchannels.

Movie. S4 Flight validation of an R3DP-printed propeller mounted on a small UAV.